Article ID: 1000-324X(2020)03-0390-09 **DOI:** 10.15541/jim20190314

Sorption Behaviors and Mechanisms of Eu(III) on Rice Straw-derived Biochar

DONG Lijia[1], WU Siying[1], LI Shengbo[1], WEI Zuofu[2], YANG Guo[1], HU Baowei[1]

(1. School of Life Science, Shaoxing University, Shaoxing 312000, China; 2. School of Life Science, Shanxi Normal University, Linfen 041004, China)

Abstract: Biochar, derived from agricultural residuals, is extensively applied to remove detrimental heavy metals from wastewater, which has dual significance for the environment protection. Herein, the sorption behavior and interaction mechanism of Eu(III) on rice straw-derived biochar was investigated by batch and spectroscopic technologies. The solution pH significantly affects the percentage of the sorption, but has little effect on the contact time. Humic substances (HA/FA) significantly enhance Eu(III) sorption with solution pH<7.0, but inhibit the sorption with solution pH>7.0. The sorption mechanism involves co-precipitation or inner-sphere surface complexation. And the chemical sorption rate is restricted by intra-particle diffusion process. Besides, the Freundlich model simulates isotherms best and the maximum sorption amount is up to 40.717 mg/kg, which correlates with the stratified structure and abundant functional groups of biochar. The thermodynamic parameters suggest that the sorption of Eu(III) on biochar is a spontaneous and endothermic process. Therefore, these results are valuable to assess the potential application values of rice straw-derived biochar for the removal of Eu(III) in water systems.

Key words: rice straw-derived biochar; Eu(III); sorption behavior; sorption mechanism; spectroscopic technology

Radioactive contamination has drawn great attention with the development of nuclear science and technology. Especially for long-lived actinides and lanthanides, even little radioactivity can pose long-term radiation for water and hazard human health[1-3]. Thus, it is vital to remove or immobilize the radionuclide from the radioactive wastewater as high-efficient as possible. Europium (Eu), as a homologue for the actinides and lanthanides due to their similar physicochemical properties and similar ionic radius, has been widely studied[1,4-8]. The research on Eu(III) is helpful for us to understand other trivalent actinides and lanthanides in the environment. Currently, many technologies were applied to remove Eu(III), such as precipitation[9-10], ion exchange[11], adsorption[1,2-4,12-13], coagulation-flocculation[14], and membrane filtration[15]. Among these approaches, sorption is a cost-efficient and widely-used method.

Generally, the sorption behavior of a radionuclide on the solid-water interface is a crucial process mediating its diffusion, migration, mobility and bio-availability in the natural environment[16-17]. For Eu(III), its sorption behavior on various absorbents such as compacted bentonite[18], alumina[19], carbon nanotubes[20], titanate nanotubes[4], manganese dioxide[6], attapulgite[21], γ-Al_2O_3[16], graphene oxide[1,8,22] has been widely studied. However, biochar, as a low-cost and highly efficient adsorbent, is a relatively new practice. Furthermore, biochar has rarely been used to remove Eu(III). For example, Frišták *et al.*[23] separated the Eu sorption on Fe-modified biochar in their recent work. Therefore, it is necessary to enhance its sorption research on biochar.

Biochar-based materials with excellent physicochemical properties and diversified functionalities are widely used in wastewater treatment fields[24]. As one of diverse feedstocks, agricultural residues are generally employed to make biochar by thermal degradation in an oxygen-limited environment[25]. Especially, herbaceous biochars usually have higher carbon contents, larger surface areas and strong aromaticity, high porosity, and abundant oxygen functional groups[24], which benefits the removal of heavy metals. In recent decades, many researchers have proved sorption mechanisms of heavy metals on biochar, including physical sorption, ion exchange, electrostatic interactions, complexation, precipitation, which endows biochar with high-efficient sorption capability[25]. For example, 99% Cd, Pb, and Zn could be removed from

Received date: 2019-06-26; **Revised date:** 2019-08-28
Foundation item: National Natural Science Foundation of China (31700476)
Biography: DONG Lijia (1984–), female, PhD, lecturer. E-mail: Donglijia@126.com
董丽佳(1984–), 女, 博士, 讲师. E-mail: Donglijia@126.com
Corresponding author: HU Baowei, professor. E-mail: hbw@usx.edu.cn
胡保卫, 教授. E-mail: hbw@usx.edu.cn

aqueous solutions by using biochar[26]. Commercial biochar shows excellent sorption performances towards several heavy metal ions, such as Zn(II), Cu(II), Co(II), Pb(II), and Cd(II)[27]. Currently, biochar is more widely researched on the sorption for some heavy metals, especially for cadmium ions, lead and chromium ions[24]. For Eu(III), it is relatively scanty. Thus, biochar technology, as a promising and emerging waste water treatment technology, should be applied to explore its sorption capability for Eu(III) from water.

All properties of adsorbates, adsorbents, and aqueous solutions determine the sorption behavior of heavy metals on adsorbents. Effects of many environmental factors such as pH, ionic strength, humic substances, and temperature on Eu(III) sorption onto various adsorbents have been proved to be evident[1-5,16-19,26]. It indicates that environmental factors of solid-liquid interface mediate the Eu(III) sorption process. For example, pH affects Eu(III) removal ratio through changing the speciation, surface charge and binding sites of the sorbents[1,19]. Humic substances enhance or inhibit the Eu(III) sorption through different degrees of complexation with adsorbates and adsorbents[5,19]. Higher temperature provides sufficient energies for the transfer of Eu(III) to the interior of the absorbent[4,19]. However, the Eu(III) sorption behavior on biochar as a function of various environmental factors is still scarcely studied. Therefore, it is necessary to explore the relative mechanism to make sure the sorption capacitiy of biochar for Eu(III).

In present work, we selected the agricultural residual (rice straw) slowly pyrolyzed at 600 ℃ as the adsorbent to investigate the effects of contact time, pH, ionic strength, humic substances, and temperature on the sorption behavior of Eu(III). To illustrate the characteristics of the adsorbent, biochar samples derived from rice straw were detected using SEM, TEM, and FT-IR, respectively. To demonstrate the interaction mechanisms between Eu(III) and the biochar, three kinetic models and four isotherm models were built.

1 Experimental method

1.1 Materials

The aboveground biomass of rice straw was harvested from Shaoxing city (Zhejiang province, China). Specifically, the rice straw was firstly obtained in the field, washed with distilled water and then dried at 105 ℃ in the lab. The dried biomass was crushed and ground to <1.0 mm particle size using a fodder grinder and then was sieved by less than 250 μm (60 mesh) sieve. Subsequently, the sieved particles were pyrolyzed at 600 ℃ with a supply of N_2 at a rate of 7 ℃/min. And to keep complete carbonization, the pyrolysis time was set at 4 h.

Eu(III) stock solution was prepared by dissolving, evaporating, and re-dissolving Eu_2O_3 in 1.0 mmol/L $HClO_4$. Humic substances，*i.e.*, humic acid (HA) and fluvic acid (FA), extracted from the soil in Hua-Jia county (Gansu province, China), were adequately studied previously and proved to have strong effects on interactions between adsorbate and adsorbent[3,28]. All chemicals employed in this experiment were purchased in analytical purity and used without any purification. All solutions were prepared with Milli-Q water.

1.2 Characterization of rice straw-derived biochar

A field emission scanning electron microscope (JSM-6360LV, Japan) and a transmission electron microscope (JEM-1011, Japan) instrument were used to observe the microstruture of rice straw-derived biochar samples, respectively. The FT-IR spectra of the biochar was recorded with a FT-IR spectrometer (NEXUS, America) in the wavelength range of 4000–400 cm^{-1} to characterize its surface functional groups. In addition, Brunauer-Emmett-Teller (BET) and Barrett-Joyner-Halenda (BJH) models were used to evaluate specific surface area and pore volume of the rice straw-derived biochar samples, respectively.

1.3 Batch sorption experiments

The batch experiments of Eu(III) on biochar were carried out at three temperatures, *i.e.*, 298, 318, and 338 K. Specifically, the stock suspensions of Eu^{3+} solution, biochar, $NaClO_4$, HA, FA, and Milli-Q water were added in polyethylene tubes in order to get the desired concentrations of different components. The ratio of Eu(III) to the solution volume was 0.45 g/L. The pH of sorption systems were adjusted through adding inappreciable volumes of 0.01 or 0.1 mol/L $HClO_4$ or NaOH solutions. The suspensions were stirred for 24 h to reach the sorption equilibrium, and then the solid and liquid phases were separated by centrifugation at 9000 r/min for 30 min.

The Eu(III) concentration in the supernatant was measured by liquid scintillation counting using a Packard 3100TR/AB Liquid Scintillation analyzer (PerkinElmer) with ULTIMA GOLD ABTM scintillation cocktail. The Eu(III) removal percent [Eu(III) sorption=$(C_0–C_e)/C_0\times 100\%$], distribution coefficient [$K_d=(C_0–C_e)/C_e\times V/m$], and sorption amount onto biochar [$q_e=(C_0–C_e)\times V/m$] were calculated from the initial Eu(III) concentration (C_0, mg/L), the final or equilibrium Eu(III) concentration (C_e, mg/L), the biochar mass (m, g), and the suspension volume (V, L).

All experimental data were subjected to the averages of duplicate or triplicate experiments to ensure the experimental repeatability and improve the data accuracy. The relative errors of the experimental data were less than 5%.

2 Results and discussion

2.1 Characterization of biochar

Fig. 1 shows SEM image, TEM image, and FT-IR spectrum of rice straw-derived biochar. SEM image suggests the stratified structure is formed and there are large gaps between two stratums (Fig. 1(a)). Furthermore, both surface and edge of each stratum are relatively rough. TEM image shows that the biochar sample has two kinds of inner structures: one is loose and rough, the other is sheet and smooth, both of which may endow the biochar with excellent sportive capability (Fig. 1(b)). FT-IR spectrum indicates functional groups on biochar (Fig. 1(c)). The band at 3444 cm^{-1} is ascribed to both free and H-bonded –OH stretching vibrations of biochar[29-30]. The peaks at 1385 and 1037 cm^{-1} are attributed to aromatic carboxyl O=C–O and alkoxy C–O stretching vibrations, respectively[1]. The bands at 795, 521, and 467 cm^{-1} are attributed to the integrated crystalline structure of biochar[31]. These oxygen functional groups may effectively bind with heavy metals. According to the results shown in our previous study[32], the average pore diameter is 45.43 nm, and the specific surface area of the biochar is 61.11 m^2/g.

2.2 Influence of pH and ionic strength

The initial solution pH importantly affects the sorption behavior of heavy metals on biochar[1,19]. The influence of pH on the Eu(III) sorption on biochar in the range of 1.9–10.2 is shown in Fig. 2(a). The sorption percentage increases from 9% to 97% with the increase of pH in the range of 1.9–8.4. In this process, the sorption increases rapidly in the pH range of 1.9–7.2, but becomes slowly at

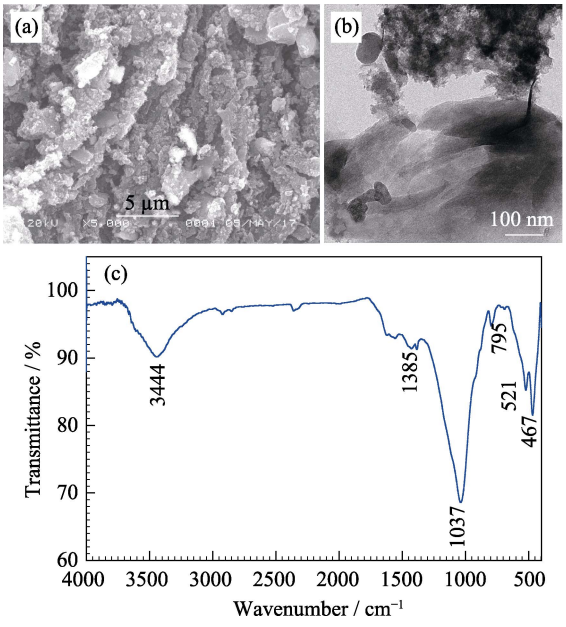

Fig. 1 SEM image (a), TEM image (b), and FT-IR spectrum (c) of rice straw-derived biochar

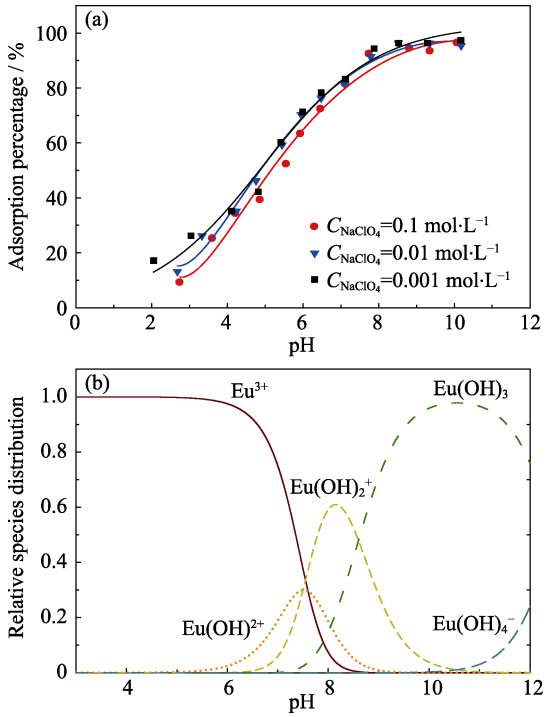

Fig. 2 Influence of ionic strength on Eu(III) sorption on biochar as a function of pH(a), and the relative distribution of Eu(III) species in solutions as a function of pH(b)
T=(298±2) K, $C_{Eu(III)initial}$=10.0 mg/L, m/V=0.45 g/L

pH>7.2. At last, the highest sorption level is maintained at pH>8.4. It indicates that Eu(III) sorption is strongly dependent on pH, which is consistent with the Eu(II) sorption on some other adsorbents such as alumina oxides[33], multiwall carbon nanotubes[34], hydrous alumina[35], and graphene oxide[1]. This phenomenon can be explained by the microstructures of Eu(III) on an adsorbent calculated from the EXAFS spectra and the species of Eu(III) on biochar surface. For example, Sheng *et al.*[4-6] found that the (co)precipitation of Eu(III) could form at high pH, which can partially explain why the sorption maintains in high level at high pH. In addition, the relative distribution of Eu(III) species at different pH calculated from the hydrolysis constants of Eu(III) is shown in Fig. 2(b). The ion Eu^{3+} is the main species at pH<7.3, and $Eu(OH)_2^+$ is the dominant species at pH 7.4–8.4. Thereby, it is reasonable that the sorption rapidly increases at pH 1.9–7.2 and slowly increases at pH 7.3–8.4. Besides, the precipitation $Eu(OH)_3$ is the dominant species at pH>8.4, so that the sorption maintains the high level. In fact, the variation of Eu(III) species at different pH is not the only reason. The surface charge and binding sites may be other reasons. According to protonation reaction (*i.e.*, $SOH+H^+ \leftrightarrow SOH_2^+$), the electrostatic repulsion can occur between Eu(III) and the positively-charged sites on biochar in the low uptake of Eu(III) due to large number of binding sites at low pH. Nevertheless, the biochar surface becomes negatively-charged at high

pH due to the deprotonation reaction (*i.e.*, $SOH \leftrightarrow SO^- + H^+$). Thereby, electrostatic repulsion significantly decreases with pH raising, which enhances the Eu(III) sorption until the formation of the Eu(III) precipitation.

Fig. 2(a) also shows the influence of three $NaClO_4$ concentrations (*i.e.*, 0.1, 0.01, 0.001 mol/L) on sorption. The sorption of Eu(III) on biochar is independent on ionic strength. In fact, the responses of the sorption to pH and ionic strength generally determine the interaction mechanism between adsorbent and adsorbate. If the sorption is affected by both pH and ionic strength, the interaction is dominated by outer-sphere complexation or ions exchange; if the sorption is affected by pH but not ionic strength, inner-sphere complexation dominates[21]. Our results show that the pH effects are significant while the effects of different ionic strength are not obvious. Thereby, inner-sphere surface complexation predominated in the sorption of Eu(III) on the biochar.

2.3 Influence of humic substances

Both FA and HA can control sorption and transport due to their strong complexation ability with metal ions[16]. Here, the presence of HA/FA enhances Eu(III) sorption on biochar at pH<7.0, but inhibits Eu(III) uptake at pH>7.0 (Fig. 3). And there is no obvious gap between HA and FA addition at the whole range of pH. The results are similar to effects of HA/FA on the sorption of Eu(III) on GO[1], γ-Al_2O_3[16], and compacted bentonite[18]. HA/FA can mediate Eu(III) sorption by changing the adsorbent surface charges and/or the sites availability[36]. The Zeta potentials for both FA and HA are negative at pH>2[35]. Interestingly, the complexation ability of surface adsorbed HA/FA with Eu(III) is stronger than that with adsorbents. Thereby, the negatively-charged HA/FA is easier adsorbed on the positively-charged biochar at low pH. While the positively-charged Eu(III) ions easily form complexes with HA/FA, which enhances Eu(III) sorption on HA/FA-biochar hybrids. At high pH, the solubility of HA/FA increases and the biochar becomes negatively-charged, leading to the electrostatic repulsion. In addition, a part of free stable HA/FA-Eu(III) complexes form in solutions. Thus, the negatively-charged HA/FA is difficult to be adsorbed on the biochar surface, resulting in the decrease of Eu(III) sorption on biochar[1,16-18].

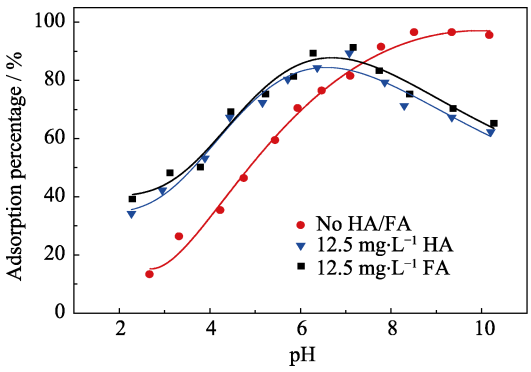

Fig. 3　Effect of HA/FA addition on Eu(III) sorption onto biochar under the conditions of T=(298±2) K, $C_{Eu(III)initial}$=10.0 mg/L, m/V=0.45 g/L, C_{NaClO_4}=0.01 mol/L

2.4 Influence of contact time

The contact time of Eu(III) uptake on biochar at 4 pH is shown in Fig. 4(a). The sorption of Eu(III) is fast at the first 2 h but becomes slowly until stable. The possible explanation is that the reactive sites on the adsorbent surface have large binding energies. At beginning, all surface sites of biochar are totally exposed resulting in an rapid increase of Eu(III) sorption. After the sites are almost occupied by Eu(III) ions, Eu(III) sorption becomes slow and diffuses into the micropore sites[37]. Notably, the contact time at 4 pH is similar, which applies that all the sorption processes under 4 pH conditions are dominated by chemical rather than physical sorption[38-39]. However, the adsorption content is enhanced by pH, which is coincident with the effects of the above-mentioned pH.

Both surface characteristics and diffusion resistance of sorbents control the sorption rate for metals. Thus, common appropriate kinetic models can uncover underlying uptake mechanisms[40]. To study the specific rate constant of Eu(III) sorption on biochar, pseudo-second order model and intra-particle diffusion model are used to fit the sorption data. The linear form of the pseudo-second order kinetic is calculated as follows[40-41]:

$$\frac{t}{q_t} = \frac{1}{kq_e^2} + \frac{t}{q_e} \quad (1)$$

where k [g/(mg·h)] is the rate constant; q_e and q_t represent the sorption ability of Eu(III) (mg/g) at equilibrium time and time t (h), respectively. The three dimensional linear plots of t/q_t *vs.* t at 4 pH are shown in Fig. 4(b). All corresponding kinetic parameters are shown in Table 1, in which the kinetic sorption process at each pH can be well described by the pseudo-second-order rate equation, because all the correlation coefficients (r^2) are close to 1.

In the processes of Eu(III) sorption on biochar, the Eu(III) shifting from biochar surface to intra-particle active sites may limit the sorption rate[42-43]. Thereby, we fit the relative intra-particle diffusion model. It can be expressed as follows[25]:

$$q_t = k_{int}\, t^{1/2} + C \quad (2)$$

where k_{int} is the intra-particle diffusion rate constant, and C represents a constant. In Table 1, r^2 for the particle diffusion model are more than 0.65, suggesting that this model fit the experimental data well. And the 3D plots of

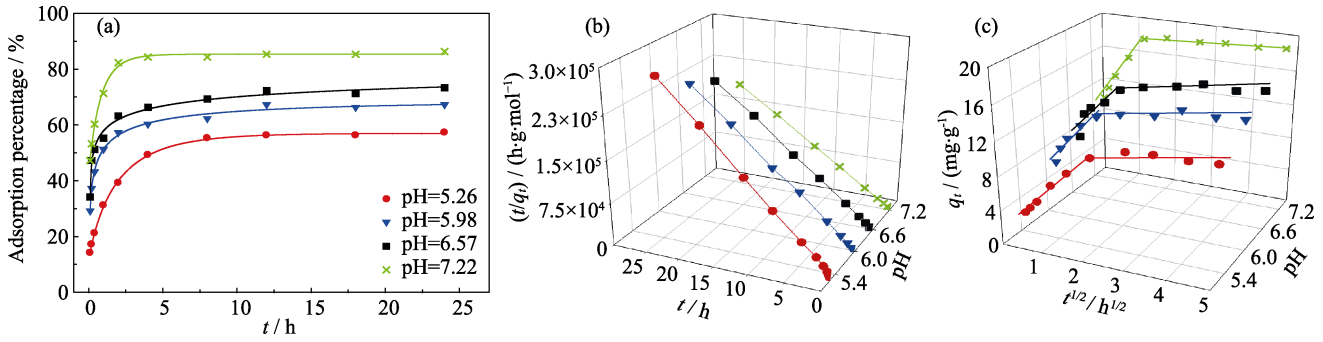

Fig. 4 Eu(III) sorption percentage on biochar as a function of contact time and pH (a), 3D plots of t/q_t *vs.* t for pseudo-second-order model simulation (b), and q_t *vs.* $t^{1/2}$ for intra-particle diffusion model simulation at 4 pH (c)
T=(298±2) K, $C_{Eu(III)initial}$=10.0 mg/L, m/V=0.45 g/L, C_{NaClO_4}=0.01 mol/L

Table 1 Parameters of Eu(III) sorption kinetic on rice straw-derived biochar with 4 pH of solutions

pH	Pseudo-second-order model			Intra-particle diffusion model	
	q_e/(mol·g^{-1})	K/(g·mol^{-1}·h^{-1})	r^2	k_{int}/(mg·g^{-1}·h$^{-1/2}$)	r^2
5.26	1.265×10^{-4}	5.361×10^{4}	1.000	2.147	0.829
5.98	1.073×10^{-4}	3.503×10^{4}	1.000	1.589	0.764
6.57	9.911×10^{-5}	3.253×10^{4}	1.000	1.513	0.749
7.22	8.591×10^{-5}	1.756×10^{4}	0.999	1.630	0.650

Under the conditions of T=(298±2) K, C_{NaClO_4}=0.01 mol/L, $C_{Eu(III)initia}$=10 mg/L, m/V=0.45 g/L

q_t *vs.* $t^{1/2}$ for intra-particle diffusion model simulation at 4 pH show that the lines do not pass through the origin (Fig.4(c)). Thus intra-particle diffusion is not the only rate control step but still exert influence on the sorption behavior of Eu(III) on biochar.

2.5 Sorption isotherms and thermodynamic study

Fig. 5 shows that the sorption isotherms of Eu(III) on biochar. The amount of Eu(III) sorption increases with temperature elevating, indicating that the temperature can promote Eu(III) sorption. To explore the sorption mechanism, we simulate sorption isotherms using 4 equilibrium models, *i.e.*, Langmuir, Freundlich, Temkin, and Dubinin-Radushkevich (D-R) model. Their linear forms are expressed as:

$$\frac{C_e}{q_e} = \frac{1}{K_L q_{max}} + \frac{C_e}{q_{max}} \quad (3)$$

$$\lg q_e = \lg k_F + n \lg C_e \quad (4)$$

$$q_e = \frac{RT}{b} \ln A + \frac{RT}{b} \ln C_e \quad (5)$$

$$\ln q_e = \ln q_{max} - \beta \varepsilon^2 \quad (6)$$

where q_{max}(mg/g) represents Eu(III) maximum sorption ability, K_L (L·mg^{-1}) is the Langmuir affinity parameter; K_F (mg^{1-n}·L^n·g^{-1}) is the Freundlich sorption capacity parameter; n is the degree of sorption dependence on equilibrium concentration; R is the universal gas constant (8.314 J·K^{-1}·mg^{-1}); T (K) is the Kelvin temperature; b is the sorption heat; A is the binding constant; β and ε are

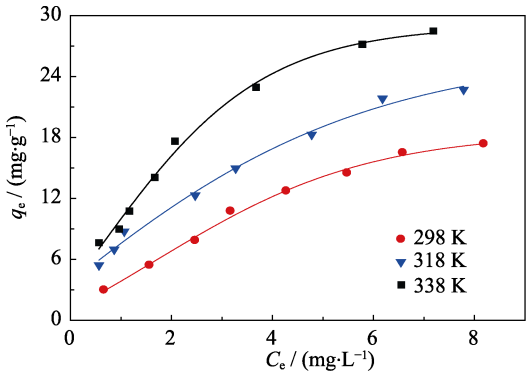

Fig. 5 Isotherms of Eu(III) sorption onto biochar at different temperatures under the conditions of pH=5.5±0.2, C_{NaClO_4}= 0.01 mol/L, m/V=0.45 g/L

the D-R activity constant and Polanyi potential, ε is calculated by $RT\ln(1+1/C_e)$. In D-R model, we also calculate the bonding energy (E, kJ/g) of the ion-exchange mechanism using the following equation:

$$E = 2\beta^{-1/2} \quad (7)$$

Fig. 6 shows the linear plots of 4 isotherm models at 3 temperatures. And their parameters are listed in Table 2. The values of r^2 imply that the four models can fit the experimental data well. From the Langmuir model, the maximum sorption amount increases from 34.626 mg/g to 40.717 mg/g with the temperature increasing (Table 2), indicating that high temperature benefits Eu(III) sorption. The n values from the Freundlich model are less than 1, and corresponding r^2 values are more than 0.97. The two results indicate that Eu(III) sorption is a nonlinear process

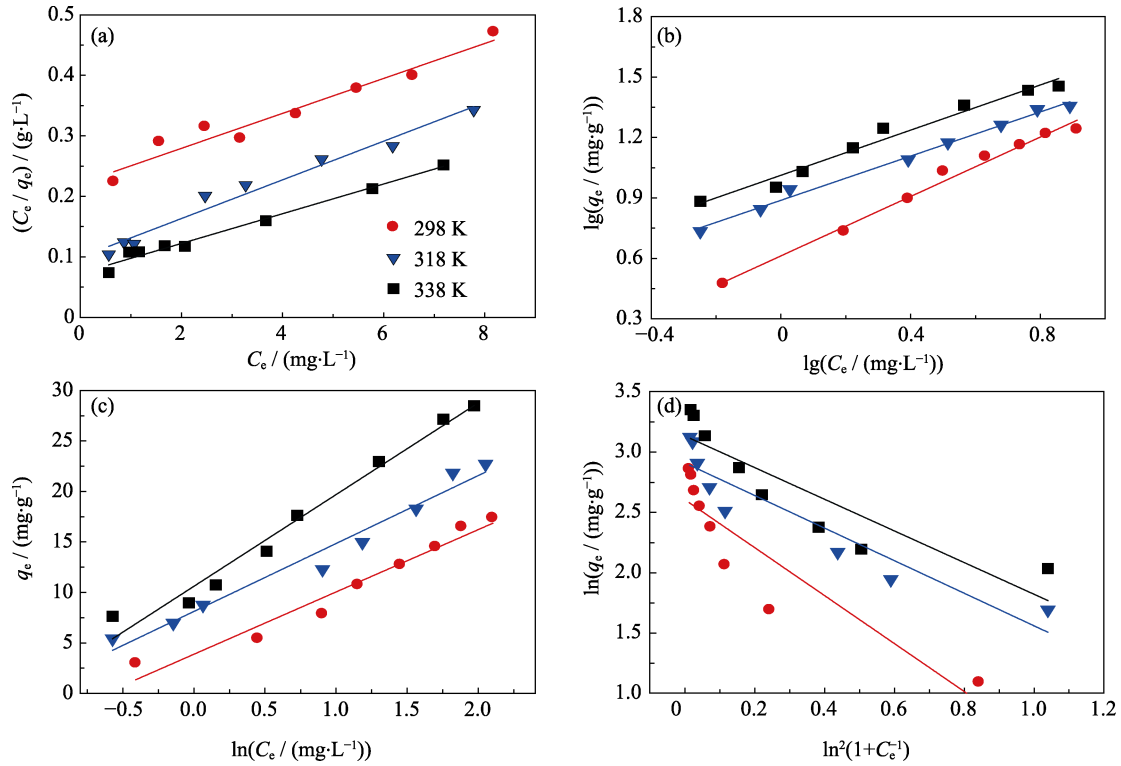

Fig. 6　Linearized Langmuir isotherm (a), Freundlich isotherm(b), Temkin isotherm (c), Dubinin-Radushkevich isotherm (d) of Eu(III) sorption on biochar at different temperatures (pH=5.5±0.2, C_{NaClO_4}=0.01 mol/L, m/V=0.45 g/L)

Table 2　Parameters for Eu(III) sorption isotherms onto rice straw-derived biochar at different temperatures

T/K	Langmuir model		
	q_{max}/(mg·g^{-1})	K_L/(L·mg^{-1})	r^2
298	34.626	0.130	0.950
318	31.289	0.322	0.974
338	40.717	0.336	0.984
	Freundlich model		
	K_F/(mg^{1-n}·L^n·g^{-1})	n	r^2
298	4.091	0.738	0.988
318	7.723	0.548	0.992
338	10.280	0.561	0.974
	Temkin model		
	A	b	r^2
298	1.875	401.551	0.957
318	3.342	374.482	0.970
338	3.217	304.874	0.978
	Dubinin-Radushkevich model		
	q_{max}/(mg·g^{-1})	E/(J·g^{-1})	r^2
298	13.518	0.502	0.824
318	18.320	0.609	0.873
338	22.920	0.617	0.801

Under the conditions of pH=5.5±0.2, $C_{Eu(III)initial}$=10 mg/L, C_{NaClO_4}=0.01 mol/L, m/V=0.45 g/L

taking place on heterogeneous biochar surface[44]. The K_F magnitude increases with the temperature elevating, suggesting that high temperature benefits Eu(III) sorption. The linear plots for the Temkin and D-R sorption isotherm also fit favorably with r^2>0.801 at 3 temperatures (Fig. 6 & Table 2). The result further supports the findings that Eu(III) sorption is a chemisorption process and enhanced by the high temperature.

Among the 4 isotherm models, the Freundlich model fits better than the other models due to the highest r^2, which implies that the Eu(III) sorption completes on heterogeneous biochar surface. The magnitude of q_{max} derived from Langmuir isotherm and D-R isotherm has a large gap, which may be arise from the different assumptions between the two isotherm formulations. Totally, these results suggest that the rice straw-derived biochar can be considered as a novel and effective adsorbent for the removal of Eu(III) from water.

To investigate the thermodynamic properties, the thermodynamic parameters (ΔH^θ, ΔS^θ, and ΔG^θ) were calculated from sorption isotherms at 3 temperatures. The free energy change (ΔG^θ) of specific sorption is calculated as[45]:

$$\Delta G^\theta = -RT \ln K^\theta \quad (8)$$

where K^θ is the equilibrium constant of sorption reaction. The values of $\ln K^\theta$ are obtained by plotting $\ln K_d$ *vs.* C_e (Fig. 7(a)). Standard entropy (ΔS^θ) and the average stan

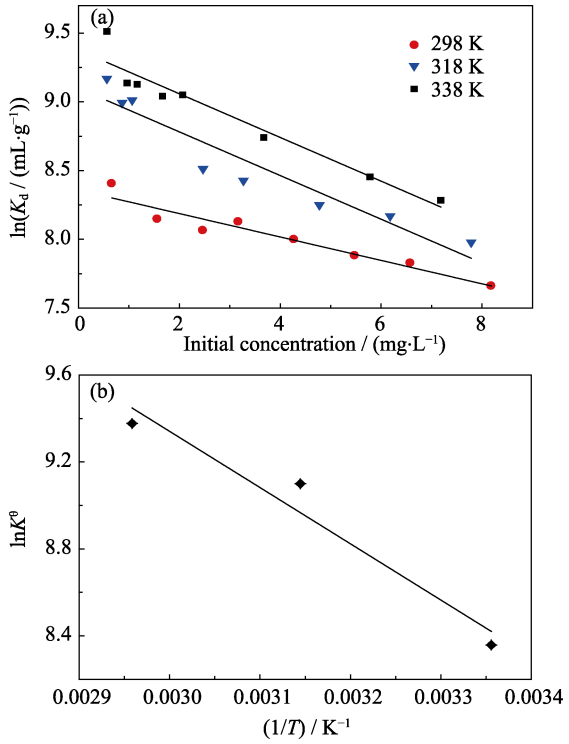

Fig. 7 Linear relationships of lnK_d *vs.* C_e for Eu(III) sorption on biochar at different temperatures (a) and ln$K^θ$ *vs.* 1/T (b). (pH= 5.5±0.2, C_{NaClO_4}=0.01 mol/L, m/V=0.45 g/L)

dard enthalpy ($\Delta H^θ$) are calculated from the slope and intercept of the plot ln$K^θ$ *versus* 1/T (Fig. 7(b)), respectively. The equation is as follows:

$$\ln(K^θ) = \Delta S^θ/\mathrm{R} - \Delta H^θ/RT \quad (9)$$

Table 3 lists the thermodynamic parameters, which is beneficial to uncover interactive mechanisms of Eu(III) and biochar. Specifically, the negative values of $\Delta G^θ$ indicate the spontaneous process of Eu(III) sorption under the experimental conditions. More negative values of $\Delta G^θ$ at higher temperature (338 K) suggest that high temperature can provide more energy for favorable sorption. The reason may be that Eu(III) are readily desolvated and its sorption are promoted at high temperature[1,13]. The positive values of $\Delta H^θ$ indicates the endothermic process of Eu(III) sorption on biochar. Also, there are strong interactions between Eu(III) and biochar. One reason is that Eu(III) has favorable solubility in solutions, and the hydration sheath of Eu(III) needs to be stripped out before its sorption on biochar. High temperature can provide more energy to favor the dehydration process. The positive value of $\Delta S^θ$ implies partial structural variations in Eu(III) and biochar during sorption process, resulting in randomness increasing of the biochar-solution interfacial system. Overall, the thermodynamic analysis illustrates that the sorption process of Eu(III) on biochar is a spontaneous and endothermic, and the sorption can be enhanced by high temperature.

Table 3 Thermodynamic parameters for Eu(III) sorption on rice straw-derived biochar at different temperatures

T/K	$\Delta G^θ$/(kJ·mg^{-1})	$\Delta S^θ$/(J·mg^{-1}·K^{-1})	$\Delta H^θ$/(kJ·mg^{-1})
298	–20.708	142.169	21.659
318	–24.059	142.169	21.151
338	–26.351	142.169	21.703

Under the conditions of pH=5.5±0.2, $C_{Eu(III)initial}$=10 mg/L, C_{NaClO_4}= 0.01 mol/L, m/V=0.45 g/L

3 Conclusions

Here, the sorption behavior of Eu(III) on rice straw-derived biochar was strongly dependent on various environmental factors, including pH, humic substances, contact time, temperature. Interestingly, the effect of each environmental factor is affected by solution pH, implying that the sorption process is complicated in natural polluted water systems, and we should consider multi-factors when remove toxic metals. According to the performance of the sorption of biochar for Eu(III), we found that surface (co)precipitation or inner-sphere surface complexation dominates the Eu(III) sorption process in the whole pH range; this chemical sorption rate was limited by intra-particle diffusion process. Furthermore, the Eu(III) sorption takes place on a heterogeneous surface of biochar which is a spontaneous and endothermic process. The research helps us to understand the sorption properties of the rice straw-derived biochar for Eu(III) and its potential application value. In future, some microscopic technologies such as XPS, EXAFS should be used to uncover the underlying mechanisms.

References:

[1] HU B, HU Q, LI X, *et al*. Rapid and highly efficient removal of Eu(III) from aqueous solutions using graphene oxide. *J. Mol. Liq.*, 2017, **229(3):** 6–14.

[2] WANG X X, YU S J, WANG X K. Removal of radionuclides by metal-organic framework-based materials. *J. Inorg. Mater.*, 2019, **34(1):** 17–26.

[3] WANG N, PANG H, YU S, *et al*. Investigation of adsorption mechanism of layered double hydroxides and their composites on radioactive uranium: a review. *Acta Chim. Sinica*, 2019, **77(2):** 143–152.

[4] SHENG G, DONG H, SHEN R, *et al*. Microscopic insights into the temperature-dependent adsorption of Eu(III) onto titanate nanotubes studied by FTIR, XPS, XAFS and batch technique. *Chem. Eng. J.*, 2013, **217(2):** 486–494.

[5] SHENG G, YANG Q, PENG F, *et al*. Determination of colloidal pyrolusite, Eu(III) and humic substance interaction: a combined batch and EXAFS approach. *Chem. Eng. J.*, 2014, **245(6):** 10–16.

[6] SHENG G, YANG S, LI Y, *et al*. Retention mechanisms and microstructure of Eu(III) on manganese dioxide studied by batch and high resolution EXAFS technique. *Radiochim. Acta*, 2014, **102(1/2):** 155–167.

[7] ZHU Y, ZHENG C, WU S, *et al*. Interaction of Eu(III) on magnetic biochar investigated by batch, spectroscopic and modeling techniques. *J. Radioanal. Nucl. Chem.*, 2018, **316(6):** 1337–1346.

[8] XIE Y, HELVENSTON E M, SHULLER-NICKLES L C, *et al*. Surface complexation modeling of Eu(III) and U(VI) interactions with graphene oxide. *Environ. Sci. Technol.*, 2016, **50(4):** 1821–1827.

[9] BURNETT J L, CROUDACE I W, WARWICK P E. Pre-concentration of short-lived radionuclides using manganese dioxide precipitation from surface waters. *J. Radioanal. Nucl. Chem.*, 2012, **292(1):** 25–28.

[10] PRAKASH D, GABANI P, CHANDEL A K, *et al*. Bioremediation: a genuine technology to remediate radionuclides from the environment. *Microb. Biotechnol.*, 2013, **6(4):** 349–360.

[11] HASSAN K F, SPELLERBERG S, SCHOLTEN B, *et al*. Development of an ion-exchange method for separation of radioiodine from tellurium and antimony and its application to the production of ^{124}I *via* the ^{121}Sb (α, n)-process. *J. Radioanal. Nucl. Chem.*, 2014, **302(10):** 689–694.

[12] SHENG G, YANG S, ZHAO D, *et al*. Adsorption of Eu(III) on titanate nanotubes studied by a combination of batch and EXAFS technique. *Sci. China Chem.*, 2012, **55(1):** 182–194.

[13] LIU X, WU J, ZHANG S W, *et al*. Amidoxime functionalized hollow carbon spheres for efficient removal of uranium from wastewater. *ACS Sustain. Chem. Eng.*, 2019, **7(6):** 10800–10807.

[14] AMBASHTA R D, SILLANPÄÄ M E. Membrane purification in radioactive waste management: a short review. *J. Environ. Radioact*, 2012, **105(2):** 76–84.

[15] KIM K W, BAEK Y J, LEE K Y, *et al*. Treatment of radioactive waste seawater by coagulation–flocculation method using ferric hydroxide and poly acrylamide. *J. Nucl. Sci. Technol.*, 2015, **53(3):** 439–450.

[16] WANG X, CHEN Z, TAN X, *et al*. Effect of pH, humic acid and addition sequences on Eu(III) sorption onto γ-Al_2O_3 study by batch and time resolved laser fluorescence spectroscopy. *Chem. Eng. J.*, 2016, **287(3):** 313–320.

[17] LIU X, SUN J, XU X, *et al*. Adsorption and desorption of U(VI) on different-size graphene oxide. *Chem. Eng. J.*, 2019, **360(3):** 941–950.

[18] WANG X, CHEN Y, WU Y. Diffusion of Eu(III) in compacted bentonite-effect of pH, solution concentration and humic acid. *Appl. Radiat. Isotopes*, 2004, **60(6):** 963–969.

[19] WANG X, XU D, CHEN L, *et al*. Sorption and complexation of Eu(III) on alumina: effects of pH, ionic strength, humic acid and chelating resin on kinetic dissociation study. *Appl. Radiat. Isotopes*, 2006, **64(4):** 414–421.

[20] TAN X L, XU D, CHEN C L, *et al*. Adsorption and kinetic desorption study of $^{152+154}$Eu(III) on multiwall carbon nanotubes from aqueous solution by using chelating resin and XPS methods. *Radiochim. Acta*, 2008, **96(1):** 23–29.

[21] CHEN Z, HE J, CHEN L, *et al*. Sorption and desorption properties of Eu(III) on attapulgite. *J. Radioanal. Nucl. Chem.*, 2016, **307(2):** 1093–1104.

[22] LIU X, MA R, WANG X, *et al*. Graphene oxide-based materials for efficient removal of heavy metal ions from aqueous solution: a review. *Environ. Pollut.*, 2019, **252(5):** 62–73.

[23] FRIŠTÁK V, MICHÁLEKOVÁ-RICHVEISOVÁ B, VÍGLAŠOVÁ E, *et al*. Sorption separation of Eu and As from single-component systems by Fe-modified biochar: kinetic and equilibrium study. *J. Iran Chem. Soc.*, 2017, **14(3):** 521–530.

[24] HUANG Q, SONG S, CHEN Z, *et al*. Biochar-based materials and their applications in removal of organic contaminants from wastewater: state-of-the-art review. *Biochar*, 2019, **1(1):** 45–73.

[25] INYANG MI, GAO B, YAO Y, *et al*. A review of biochar at a low-cost adsorbent for aqueous heavy metal removal. *Crit. Rev. Env. Sci. Tec.*, 2015, **46(2):** 406–433.

[26] KLOSS S, ZEHETNER F, DELLANTONIO A, *et al*. Characterization of slow pyrolysis biochars: effects of feedstocks and pyrolysis temperature on biocharproperties. *J. Environ. Qual.*, 2012, **41(4):** 990–1000.

[27] KOŁODYŃSKA D, KRUKOWSKA J, THOMAS P. Comparison of sorption and desorption studies of heavy metal ions from biochar and commercial active carbon. *Chem. Eng. J.*, 2017, **307(1):** 353–363.

[28] SHENG G, LI J, SHAO D, *et al*. Adsorption of copper(II) on multiwalled carbon nanotubes in the absence and presence of humic or fulvic acids. *J. Hazard. Mater.*, 2010, **178(1/2/3):** 333–340.

[29] KIM W K, SHIM T, KIM Y S, *et al*. Characterization of cadmium removal from aqueous solution by biochar produced from a giant *Miscanthus* at different pyrolytic temperatures. *Bioresource Technol.*, 2013, **138(6):** 266–270.

[30] TONG X J, LI J Y, YUAN J H, *et al*. Adsorption of Cu(II) by biochars generated from three crop straws. *Chem. Eng. J.*, 2011, **172(2/3):** 828–834.

[31] ZONG P, WANG H, PAN H, *et al*. Application of NKF-6 zeolite for the removal of U(VI) from aqueous solution. *J. Radioanal. Nucl. Chem.*, 2013, **295(3):** 1969–1979.

[32] DONG L, CHANG K, WANG L, *et al*. Application of biochar derived from rice straw for the removal of Th(IV) from aqueous solution. *Sep. Sci. Technol.*, 2018, **53(10):** 1511–1521.

[33] YANG S, SHENG G, MONTAVON G, *et al*. Investigation of Eu(III) immobilization on γ-Al_2O_3 surfaces by combining batch technique and EXAFS analysis: role of contact time and humic acid. *Geochim. Cosmochim. Acta*, 2013, **121(11):** 84–104.

[34] CHEN C, WANG X, NAGATSU M. Europium adsorption on multiwall carbon nanotube/iron oxide magnetic composite in the presence of polyacrylic acid. *Environ. Sci. Technol.*, 2009, **43(7):** 2362–2367.

[35] TAN X, WANG X, GECKEIS H, *et al*. Sorption of Eu(III) on humic acid or fulvic acid bound to hydrous alumina studied by SEMEDS, XPS, TRLFS and batch techniques. *Environ. Sci. Technol.*, 2008, **42(17):** 6532–6537.

[36] PAN D, FAN Q, LI P, *et al*. Sorption of Th(IV) on Na-bentonite: effects of pH, ionic strength, humic substances and temperature. *Chem. Eng. J.*, 2011, **172(2/3):** 898–905.

[37] LI Y, SHENG G, SHENG J. Magnetite decorated graphene oxide for the highly efficient immobilization of Eu(III) from aqueous solution. *J. Mol. Liq.*, 2014, **199(11):** 474–480.

[38] WANG X X, YANG S B, SHI W Q, *et al*. Different interaction mechanisms of Eu(III) and ^{243}Am(III) with carbon nanotubes studied by batch, spectroscopy technique and theoretical calculation. *Environ. Sci. Technol.*, 2015, **49(19):** 11721–11728.

[39] WANG X, LU S, CHEN L, *et al*. Efficient removal of Eu(III) from aqueous solutions using super-adsorbent of bentonite-polyacrylamide composites. *J. Radioanal. Nucl. Chem.*, 2015, **306(2):** 497–505.

[40] HO Y S. Review of second-order models for adsorption systems. *J. Hazard. Mater.*, 2006, **136(3):** 681–689.

[41] HO Y S, MCKAY G. Pseudo-second order model for sorption processes. *Process Biochem.*, 1999, **34(5):** 451–465.

[42] IJAGBEMI C O, BAEK M H, KIM D S. Montmorillonite surface properties and sorption characteristics for heavy metal removal from aqueous solutions. *J. Hazard. Mater.*, 2009, **166(1):** 538–546.

[43] YANG S, HU J, CHEN C, *et al*. Mutual effects of Pb(II) and humic acid adsorption on multiwalled carbon nanotubes/polyacrylamide

composites from aqueous solutions. *Environ. Sci. Technol.*, 2011, **45(8):** 3621–3627.

[44] BISWAS K, SAHA S K, GHOSH U C. Adsorption of fluoride from aqueous solution by a synthetic iron(III)-auminum(III) mixed oxide. *Ind. Eng. Chem. Res.*, 2007, **46(16):** 5346–5356.

[45] LI J, ZHANG S, CHEN C, *et al*. Removal of Cu(II) and fulvic acid by graphene oxide nanosheets decorated with Fe_3O_4 nanoparticles. *ACS Appl. Mater. Interfaces*, 2012, **4(9):** 4991–5000.

稻草生物炭对铕的吸附行为及机理研究

董丽佳[1], 吴思颖[1], 李生波[1], 魏作富[2], 杨 国[1], 胡保卫[1]

(1. 绍兴文理学院 生命科学学院, 绍兴 312000; 2. 山西师范大学 生命科学学院, 临汾 041004)

摘 要: 以农业残留物为原料制备的生物炭被广泛应用于去除重金属, 这对于环境保护具有双重意义。本研究以稻草为原料制备了生物炭, 通过系列静态实验和光谱技术研究其对重金属铕(Eu)的吸附行为及机理。研究发现溶液 pH 显著影响生物炭对 Eu(III)的吸附量, 但不改变吸附反应时间; 腐殖酸/富里酸(HA/FA)在 pH<7.0 的溶液中能促进生物炭对 Eu(III)的吸附, 而在 pH>7.0 的溶液中则抑制 Eu(III)的吸附; 吸附过程主要涉及共沉淀或内表面络合机制; 该吸附属于化学吸附, 且吸附速率受内颗粒扩散过程的限制。此外, Freundlich 模型对该吸附拟合最好, Langmuir 模型显示稻草生物炭对 Eu(III)的最大吸附量为 40.717 mg/kg, 这可能与生物炭的层状结构和丰富的官能团有关; 热力学分析表明该吸附是自发的吸热过程。这些发现有利于评估稻草生物炭在去除水中重金属方面潜在的应用价值。

关 键 词: 稻草生物炭; Eu(III); 吸附行为; 吸附机理; 光谱技术

中图分类号: TQ174 **文献标识码:** A